

Transparent glass-windowed ultrasound transducers

Torstein Yddal^{*†}, Spiros Kotopoulos^{†*}, Odd Helge Gilja^{*‡}, Sandy Cochran[§] and Michiel Postema[†]

^{*}National Centre for Ultrasound in Gastroenterology, Haukeland University Hospital,
Jonas Lies vei 65, 5021 Bergen, Norway

[†]Department of Physics and Technology, University of Bergen, Allégaten 55, 5007 Bergen, Norway

[§]Institute for Medical Science and Technology, University of Dundee, Wilson House,
1 Wurzburg Loan, Dundee Medipark, Dundee DD2 1FD, UK

[‡]Department of Clinical Medicine, University of Bergen, Jonas Lies vei 65, 5021 Bergen, Norway

Abstract—Glass windowed ultrasound transducers have several potential uses ranging from multi-modal research (ultrasound and optics) to industrial application in oil and gas or chemistry.

In our work here we compare four different designs for transparent glass windowed ultrasound transducers. Each design was characterised using field scanning, radiation force measurements, frequency sensitivity measurement and FEM simulations.

Field scans showed that small variations in design can greatly affect the size and location of the acoustic focus. The results coincided with those seen in the simulations. Radiation force measurements showed that the devices were able to easily exceed acoustic powers of 10 W, with efficiencies of up to 40%. Isostatic simulations shows that the design also affects the physical strength of the devices. Current designs were able to withstand between 300 and 700 psi on the front surface.

The devices were cost effective due to the minimal amount of materials necessary and the simple fabrication process. More work needs to be done to improve the power output and stress handling capabilities.

I. INTRODUCTION

Optical measurements are a cornerstone of today's technology, they are widely used for measuring speed and distance, performing chemical analysis, and more [1], [2]. Optical equipment draws great advantages from modern micro-electronics knowledge, making it extremely compact. Nevertheless, optical equipment tends to be very susceptible to physical damage hence needs to be shielded and requires an optically clear path, *e.g.*, a glass window. Some environments makes this difficult to obtain, for example measurements in oil pipes where crude oil will attach to the optical measurement window. Ultrasound is also used in several chemical production techniques to homogenise emulsions, and optical spectroscopy is required to evaluate the quality of the emulsion. Currently such problems are solved by measuring after emulsification and evaluating the quality of the finished product [3].

In our work here, we aim to solve such problems by creating an optically transparent transducer. The cavitation effects of the ultrasound can be used to clean the optical window or homogenise emulsions, whilst the optically clear path allows a vast range of optical based measurements, from spectroscopy, to high-frame rate imaging cameras, or optical microscopy. These optically transparent transducers need to be able to

handle high isostatic pressures, as in oil and gas pipelines the pressures may reach 1000 psi [4]. The transducers need to be able to withstand acidic corrosion, *e.g.* in harsh chemical environments, and they need to be powerful enough to induce inertial cavitation.

We evaluated several geometric designs to see the effect on the acoustic output and evaluate the ability to handle isostatic pressures via finite element modelling simulations.

II. MATERIALS AND METHODS

A. Design

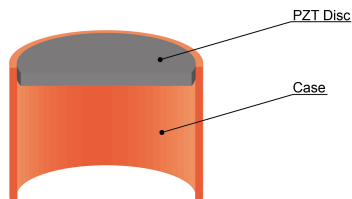
Typical ultrasound transducers are fabricated from a single piezoelectric disc to generate acoustic pressure waves, or use a bolt-clamped Langevin type design to generate mechanical motion [5]. The transparent glass windowed ultrasound transducers took advantages from both types of transducers designs. A low frequency (300-kHz) piezoelectric ring was used in place of the disc. A low frequency was used as it is easier to generate cavitation at lower frequencies. The hole in the middle of the ring was sealed, then a glass disc was bonded to the surface of the piezoelectric ring. A glass disc was used as it is low cost, has the best optical clarity compared to plastics, has a higher yield strength and resists erosion (chemical and cavitation induced) well. In addition the glass could be replaced with stronger equivalent materials such as sapphire.

Four designs variations were fabricated and evaluated (*c.f.* Figure 1). A minimum of two of each design were made to evaluate consistency between devices. Table I shows the dimensions of these designs.

B. Fabrication

The transducers were fabricated using an established process with minor variations [6]. The piezoelectric material of choice was Pz26 with silk screen printed silver electrodes (Meggit, PLC, Christchurch, United Kingdom) due to its low losses and high mechanical quality factor. Designs 1, 3 and 4 were fabricated by first aligning and bonding the glass disc (H. Baumbach & Co Ltd, Suffolk, United Kingdom) to the Pz26 ring using epoxy (EpoFix, Struers A/S, Ballerup, Denmark) and left to dry for 24 hours under a 2-kg weight. The central hole in the Pz26 ring was filled with modelling putty to ensure no epoxy seeped into the optical window. Excess epoxy

A. Traditional Transducer



B. Glass windowed Transducers

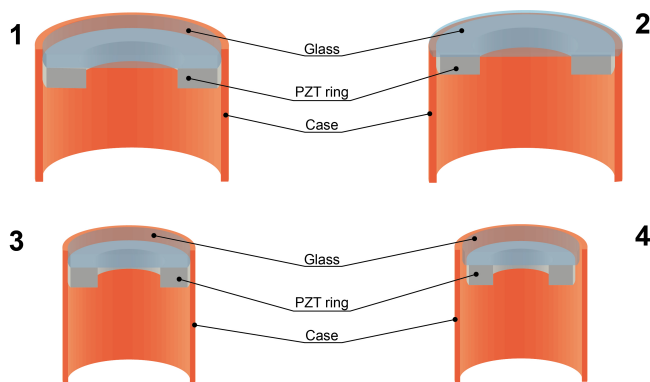


Fig. 1. Graphical representation showing the construction of (A.) a traditional transducer and (B. four different transparent transducer designs.)

87 between the PZT-ring and glass disc was removed using a
 88 scalpel to access the printed surface electrode of the PZT-ring.
 89 A microcoaxial cable was bonded using conductive Ag-epoxy
 90 (Agar Scientific, Essex, United Kingdom) as a side connection
 91 on the PZT-glass interface and on the back electrode of the
 92 PZT-ring. The microcoaxial cable was subsequently soldered
 93 to a larger diameter 50-Ω RG174 cable for increased stability
 94 and reliability. The stacked PZT-glass disc was then placed
 95 centrally in an aluminium cylinder and bonded to adhesive
 96 UV tape (Adwill D, LINTEC, Tokyo, Japan). The interface
 97 between the PZT-glass stack and aluminium cylinder was then
 98 bonded with Epofix epoxy and left to cure for 24 hours. The
 99 RG174 cable threaded through a 3-mm hole drilled into the
 100 aluminium case wall. The back side of the case was sealed
 101 with a polycarbonate disc. Bonding and sealing was achieved
 102 using generic 5-minute epoxy.

103 Design 2 was fabricated in a similar manner. The PZT
 104 ring was first bonded to the aluminium case, and the front
 105 face was connected to the aluminum case with silver paint
 106 (Agar Scientific, Essex, United Kingdom) and the glass disc
 107 was bonded to both the PZT and aluminium case. (Instead
 108 of bonding the earth of the coaxial cable to the ring itself,
 109 it was now bonded to the aluminum case). All other steps
 110 remained the same. Table I shows the dimensions of the
 111 different designs.

TABLE I
 TRANSPARENT GLASS WINDOWED ULTRASOUND TRANSDUCERS
 DIMENSIONS. ALL UNITS ARE IN MM. (KEY: ID - INNER DIAMETER, OD -
 OUTER DIAMETER, TH - THICKNESS, H - HEIGHT)

Design	PZT			Glass		Case		
	ID	OD	TH	OD	TH	ID	OD	H
1	20	40	5	40	4	44.5	51	50
2	20	40	5	50	2	44.5	51	50
3	10	25	4	25	3	31.5	38	50
4	10	25	4	30	3	31.5	38	50

C. Characterization

Field scans were performed to visualise the acoustic
 propagation pattern. The acoustic power was measured using
 a radiation force balance and frequency characterizations were
 performed to measure the bandwidth of the devices.

1) *Field scan*: The ultrasound field was inspected using
 a closed loop, custom made 3D-scanning system using a
 200-μm hydrophone. The z -axis was denoted as the acoustic
 propagation direction, and the x - and y -axis are the lateral
 and elevation directions, respectively. For each transducer 3
 different scans were performed. Two in the xy -plane, one in
 the focus of the transducer, and one, < 1-mm away from the
 front surface of the transducer. The third scan was performed
 in the yz -plane including the entire near field of the transducer
 in addition to the focus.

2) *Frequency Characterization*: The frequency response
 of the transducers were characterized using a pulse-response
 method.

The transducers were characterised between 100 kHz and
 1 MHz with a frequency step size of 1 kHz. The bandwidth in
 percentage was then calculated by

$$BW\% = \frac{f_c}{f_{6dB+} - f_{6dB-}} \cdot 100\%, \quad (1)$$

where f_c is the centre frequency, f_{6dB+} and f_{6dB-} are the
 upper and lower frequency cut-off points; -6 dB left and right
 of f_c , the frequency with the maximum sensitivity. The $+$ and
 $-$ sign indicate that the frequency is higher and lower than
 the centre frequency, respectively.

3) *Power and Pressure Characterization*: The power output
 of the transducer were measured using an absolute calibration
 technique with a radiation force balance, based on the standard
 IEC 61161 [7]. The setup used was based on a “weigh-all”
 approach, which uses an acoustic absorber (Aptflex F28,
 Precision Acoustics Ltd, Dorset, United Kingdom) attached
 to a precision scale. The acoustic power can be calculated by

$$P = c \cdot F = c \cdot m \cdot g, \quad (2)$$

where P is the acoustic power, F is the acoustic force exerted
 on the absorber, c is the speed of sound in water, m is the
 weighed “acoustic mass”, and g is the gravitational constant.

The powers were measured for multiple input electrical
 powers, and were subsequently plotted against the output
 voltage from the waveform generator.

The pressure was calculated by

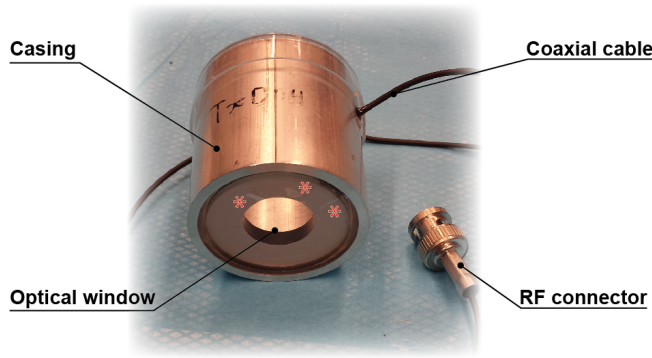


Fig. 2. Photograph showing final construction of prototype glass windowed ultrasound transducer based on Design 1. Red stars indicate bonding defects.

$$p = \frac{F}{A} = \frac{P}{c \cdot A}, \quad (3)$$

where p is the calculated pressure, and the area A of the acoustic focus at 6-dB. Whilst this was not the ideal method to estimate the pressures, it gave a rough estimate to compare performance.

4) *Simulations:* Finite element modelling (FEM) simulations were performed using Solidworks 2014 simulation (Dassault Systèmes, Velizy Villacoublay, France). An isostatic pressure load was applied across the whole front surface of the transducers, whilst the outer surface of the case was fixed. Failure points were when the stress in any of the materials exceeded the tensile modulus. Acoustic simulations were performed using PzFlex 2014 (Weidlinger Associates Inc., New York, NY).

III. RESULTS AND DISCUSSION

Figure 2 shows an example of a prototype transparent glass windowed ultrasound transducer. This transducer is based on Design 1. The optical window can be seen in the centre of the device. The device was driven by a single RF power supply. The stars indicate minor bonding defects, *i.e.*, air pockets stuck due to inhomogeneities in the PZT surface. Whilst these defects were minor, they did have an effect on the acoustic profile (*c.f.* Fig. 3). These defects resulted in acoustic “dead spots”, affecting the shape of the acoustic focus. These air pockets could be resolved by placing the device in a vacuum chamber prior to curing, or applying a stronger force during curing.

Figure 3 shows a typical response from the 3D field scan. The field scans showed that the acoustic propagation pattern was very similar to traditional ultrasound transducers, yet the different constructions affected the focal distance and sidelobes. The acoustic focus of design 1, was seen at around 81-mm from the front face of the transducer. An extremely long focal length of 111 mm can be seen. The near field shows typical behaviour, similar to that expected from a traditional piston type ultrasound transducer. A slight asymmetry can be seen, possibly due to the bonding defects described earlier.

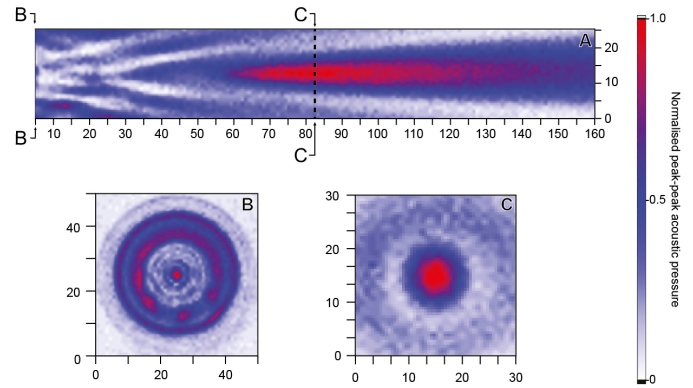


Fig. 3. 2D scans of the acoustic field of the transducer with Design 1.

TABLE II
SUMMARY OF OUTPUT PROPERTIES FROM DIFFERENT GLASS WINDOWED ULTRASOUND TRANSDUCERS.

Design	f_c (kHz)	BW (%)	Power efficiency (%)	Pressure output per W (kPa/W)	Focal distance (mm)	Focal Length (mm)
1	465	71	13	92	81	111
2	358	77	12	143	11	26
3	615	36	40	312	34	153
4	630	37	43	478	39	100

The location of these bonding-defects can clearly be seen in Fig. 3B where there are several breaks in the high pressure areas (red) in the concentric rings. A single high pressure point can be seen at the centre of the glass disc/PZT ring. This may indicate that the glass behaves as some sort of oscillating diaphragm, a desired effect. This would ensure pressure peak at the centre of the ultrasound transducer on the front face increasing the amount of cavitation based cleaning in the desired location. The acoustic focus was perfectly spherical with a pseudo-Gaussian pressure distribution (*c.f.* Fig. 3C). Only minor side lobes were visible.

Table II summarises the acoustic outputs of the four designs. The two larger devices had a lower centre frequencies of 358 kHz and 465 kHz with mean bandwidths of 74%. The power efficiency of the devices was at 13%, with a theoretical maximum of 50%. The location of the acoustic focus, and size, between the two devices was significantly different, with Design 1 having a long, distant focus, and Design 2 having a short focus, extremely close to the front face of the device. Designs 3 and 4 were much more similar with only 15 kHz difference in centre frequency, a bandwidth of 36% and efficiencies of 42%. The significant difference between these two designs was the size of the acoustic focus. Design 3 has a focal length of 153 mm; 50% larger than Design 2. The low power output may be due to the mismatch of acoustic impedances between PZT, glass, and water.

Figure 4 shows the acoustic power output as a function of waveform generator voltage. Design 3 and 4 shows a significantly higher output power when compared to Designs

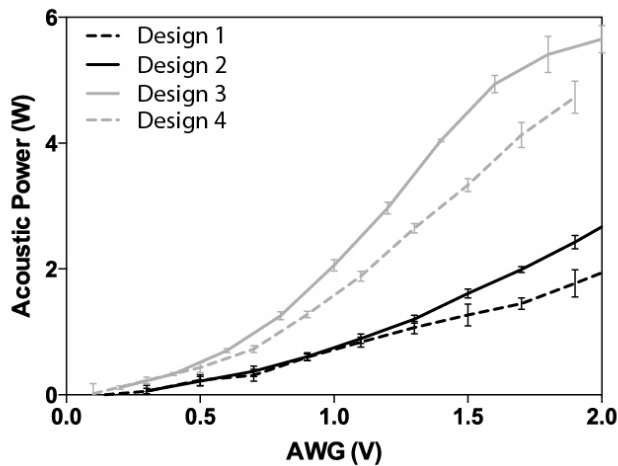


Fig. 4. Acoustic power output of various designs when driven at their resonance frequencies measured via a radiation force balance.

1 and 2. This may be due to electrical impedance mismatch between amplifier and load. The slight increase in output power of Design 2 when compared to Design 1 may be due to the thinner glass used, reducing acoustic attenuation.

Preliminary results showed that all devices were able to induce inertial cavitation, not only at the centre frequency, but also at sub-harmonics and over harmonics.

Table III summarises the simulated failure points of the different designs due to external isostatic pressures. In Designs 1 and 2, where the optical aperture was largest, the glass was seen to fail first. Design 1 failed at around 700 psi, where as Design 2 failed at 300 psi. This is due to the thinness of the glass in Design 2, hence glass thickness plays a large role in the strength of the devices. Design 3 and 4 both failed at around 500 psi. In contrast with Design 1 and 2, the piezoelectric material failed first. As the ratio of optical window size to glass thickness was significantly larger than Designs 1 and 2, the glass was able to deform more yet distribute the stress better. Nevertheless, the stress was then distributed into the PZT, which has a lower tensile strength than glass inducing early failure.

TABLE III
ISOSTATIC PRESSURE SIMULATIONS.

Design	Failure Material	Failure pressure [Psi]
1	Glass disk	700
2	Glass disk	300
3	PZT-ring	500
4	PZT-ring	500

In oil and gas pipelines, the pressure may vary between 300 and 1000 psi, hence there is potential for such devices [4].

Acoustic simulations (data not shown) showed near identical results when compared to the measured values in terms of acoustic propagation pattern.

5) *Future Perspectives:* A primary issue during fabrication was ensuring a perfect bond. Air pockets (*c.f.* Fig.2) can get trapped between the glass and PZT. This adhering process needs to be optimised to extract all possible air pockets. Placing the device in a vacuum may help extract the trapped air.

The glass used did not have an optimised thickness, hence destructive interference may be occurring in the glass. Using quarter wavelength thick glass, or odd multiple of would greatly improve the efficacy of the devices. In addition electrical impedance matching would greatly help reduce electrical reflections.

A major issue with the current design was thermal degradation. When running continuously in excess of 100 W input power, the PZT would overheat and de-polarise. Adding active cooling would resolve such issues.

As both simulations show promise, in future, such designs will be simulated and virtually optimised to match all the necessary criteria prior to fabrication.

IV. CONCLUSION

Fabricating high-power transparent windowed ultrasound transducers is feasible at a low cost. Early prototypes have shown that the design can drastically vary the electric and acoustic profile of the devices. Simulations shows that it is possible to predict the acoustic profile and that the designs have potential for use in high-pressure environments. Such devices may have many applications in the field of both research and industry. Nevertheless, these devices are only prototypes and there is vast room for improvement.

ACKNOWLEDGEMENTS

This study has been supported by MedViz (<http://medviz.uib.no/>), an interdisciplinary research cluster from Haukeland University Hospital, University of Bergen, and Christian Michelsen Research AS. The authors would like to thank The Michelsen Centre for Industrial Measurement Science and Technology for their support throughout this project.

REFERENCES

- [1] M.-C. Amann, T. Bosch, M. Lescure, R. Myllyla, and M. Rioux, "Laser ranging: a critical review of usual techniques for distance measurement," *Opt. Eng.*, vol. 40, no. 1, p. 10, 2001.
- [2] J. López-Higuera, "Fiber optic sensors in structural health monitoring," *J. Light. Technol.*, vol. 29, no. 4, pp. 587–608, 2011.
- [3] R. Stöckle, Y. Suh, V. Deckert, and R. Zenobi, "Nanoscale chemical analysis by tip-enhanced Raman spectroscopy," *Chem. Phys. Lett.*, vol. 318, no. 1, pp. 131–136, 2000.
- [4] T. Miesner and W. Leffler, *Oil & gas pipelines in nontechnical language*, 2006.
- [5] K. Adachi and M. Saito, "Construction of Torsional-Vibration Systems with a Hollow Cylindrical Bolt-Clamped Langevin-Type Transducer and Their Application to Ultrasonic Plastic Welding," *Jpn. J. Appl. Phys.*, vol. 34, no. Part 1, No. 5B, pp. 2735–2739, May 1995.
- [6] S. Kotopoulos, H. Wang, S. Cochran, and M. Postema, "Lithium niobate ultrasound transducers for MRI-guided ultrasonic microsurgery," *IEEE Trans. Ultrason. Ferroelectr. Freq. Control*, vol. 58, no. 8, pp. 1570–1576, 2011.
- [7] International Electrotechnical Commission, "Ultrasonics - Power measurement - Radiation force balances and performance requirements," Tech. Rep., 2013.